Proton decay of excited states in ^{12}N and ^{13}O and the astrophysical ^{11}C(p,γ)^{12}N reaction rate

L. G. Sobotka,[1] W. W. Buhro,[1] R. J. Charity,[1] J. M. Elson,[1] M. F. Jager,[1] J. Manfredi,[1] M. H. Mahzoon,[1] A. M. Mukhamedzhanov,[2] V. Eremenko,[2] M. McCleskey,[2] R. G. Pizzone,[2,*] B. T. Roeder,[2] A. Spiridon,[2] E. Simmons,[2] L. Trache,[2,†] M. Kurokawa,[3] and P. Navrátil[4]

[1]*Departments of Chemistry and Physics, Washington University, St. Louis, Missouri 63130, USA*

[2]*Cyclotron Institute, Texas A&M University, College Station, Texas 77843, USA*

[3]*RIKEN Nishina Center, Wako, Saitama 351-0198, Japan*

[4]*TRIUMF, 4004 Westbrook Mall, Vancouver BC, V6T 2A3, Canada*

(Received 4 April 2013; published 23 May 2013; corrected 6 June 2013)

Using a ^{13}O beam, we have observed proton decays of ^{12}N and ^{13}O excited states following proton-knockout and inelastic interactions on a ^{9}Be target. The excited states were determined from detected two- and three-body exit channels using the invariant mass method. The width of the second excited state of ^{12}N was determined to be 55(20) keV, considerably smaller than the value listed in the ENSDF data base. Three new excited states of narrow width ($\Gamma < 50$ keV) were observed in ^{13}O from the $p + {}^{12}$N and $2p + {}^{11}$C exit channels. One of these states ($E^* = 3.67$ MeV) was found to sequentially decay to the second excited of ^{12}N. We again found these data to be inconsistent with the listed decay width. The ramifications for the astrophysically interesting ^{11}C(p,γ)^{12}N reaction are given.

DOI: 10.1103/PhysRevC.87.054329 PACS number(s): 27.20.+n, 23.50.+z, 26.20.Np, 26.30.−k

I. INTRODUCTION

Information on the excited states of ^{13}O is quite sparse. Using the ^{12}C(p,π^-)^{13}O reaction, Couvert *et al.* found an excited state at $E^* = 2.82(24)$ MeV [1]. Subsequently, Seidl *et al.* employing the ^{13}C(π^+,π^-)^{13}O reaction, found levels at $E^* = 2.75(4)$ MeV, 4.21 MeV, and 6.02(8) MeV [2]. No other information such as spins or decay widths were presented in these early studies. More recently, Skorodumov *et al.* used resonance $p + {}^{12}$N elastic scattering to determine the properties of the first excited state [$E^* = 2.69(5)$ MeV, $J^\pi = 1/2^+$, and $\Gamma = 0.45(10)$] [3]. The energy of this state is consistent with the 2.75-MeV state of Seidl *et al.* and the single state of Couvert *et al.* In addition, Skorodumov *et al.* found evidence for another state at $E^* = 3.29$ MeV with $J^\pi = (1/2^-,3/2^-)$ and $\Gamma = 0.075(3)$ MeV.

Compared to its mirror nucleus ^{13}B, the first excited state in ^{13}O is ∼0.8 MeV lower in energy. This was interpreted as a Thomas-Ehrman effect associated with occupancy of the loosely bound $1s_{1/2}$ single-particle level [3]. For the second excited state in ^{13}B at 3.53 MeV, Iwasaki *et al.* found evidence for a dominant intruder ($\nu 2p2h$) configuration [4]. Thus we expect the *sd* shell is important for understanding the excitations of ^{13}O.

The present work finds two additional levels in ^{13}O well below the first excited state in ^{13}B. This raises the question of how the strength of the $1s_{1/2}$ single-particle level is distributed. From a more global perspective, the study of the $|T_z| = 3/2$ members of the $A = 13$ isobar adds to the richness of the classic isospin symmetry breaking due to the effect of an encroaching continuum first studied in the $|T_z| = 1/2$ members of this isobar,^{13}C and ^{13}N [5,6].

The present work also provides a new width of the second excited state in ^{12}N. This revised width has nucleosynthetic implications. While the $3\alpha \rightarrow {}^{12}$C reaction is the traditional way to connect the *p*-*p* chains to CNO in most astrophysical environments, in some particular environments, this process might be bypassed by a number of reaction sequences suggested by Wiescher *et al.* [7]. Two of these sequences called rap-II and rap-III, respectively, are

$$^{7}\mathrm{Be}(\alpha,\gamma)^{11}\mathrm{C(p,}\gamma)^{12}\mathrm{N(p,}\gamma)^{13}\mathrm{O}(\beta^+,\nu)^{13}\mathrm{N(p,}\gamma)^{14}\mathrm{O},$$
$$^{7}\mathrm{Be}(\alpha,\gamma)^{11}\mathrm{C(p,}\gamma)^{12}\mathrm{N}(\beta^+,\nu)^{12}\mathrm{C(p,}\gamma)^{13}\mathrm{N(p,}\gamma)^{14}\mathrm{O}.$$

The creation of early CNO material before the triple-α flux builds up may be important in the evolution of massive stars with low metallicity. This material could be the seeds of the CNO cycle and would lead to increased energy release. Even very small amounts of CNO material could make a significant difference in some situations [8–10].

Both the rap-II and rap-III sequences involve the ^{11}C(p,γ)^{12}N reaction and a number of theoretical and experimental efforts have been made to determine the energy dependence of the reaction cross section [7,11–16]. Because of the low Q value, direct capture to the ground state is very significant, however, resonant capture through low-lying excited states (as well as interference between direct and resonant processes) must also be considered. These contributions require knowledge of the properties of the low-lying states of ^{12}N.

The first excited state of ^{12}N is narrow, thus not only is its contribution localized in energy but it also contributes little to the overall uncertainty of the (p,γ) capture rate. On the other hand, the second excited state of ^{12}N has a large and uncertain width. The width of this $J^\pi = 2^-$ state at $E^* = 1.18$ MeV is listed as 118(14) keV in the ENSDF data base [17]. This value, however, is an average of a number of experimental

[*]Permanent address: INFN, Laboratori Nazionali del Sud, Catania, Italy.

[†]Currently on leave: National Institute of Physics and Nuclear Engineering "Horia Hulubei" Bucharest-Magurele, R-77125, Romania.

TABLE I. Summary of properties for level observed in this work.

Nucl.	E^* (MeV)	Γ (keV)	J^π (MeV)	Ratio	Branch
^{12}N	1.179(17)[a]	55(20)	2^-	100%	$p+{}^{11}C_{g.s.}$
^{13}O	2.956(20)[b]	<50		∼100%	$p+{}^{12}N_{g.s.}$
^{13}O	3.025(16)[c]	<50		∼100%	$p+{}^{12}N_{1st}$
^{13}O	3.669(13)	<50		10(2)%	$p+{}^{12}N_{1st}$
				90(2)%	$p+{}^{12}N_{2nd}$

[a]Average of Breit-Wigner and *R*-matrix fits.
[b]If this and the next entry are one state, this branch is 29(8)%.
[c]if this and the previous entry are one state, this branch is 71(8)%.

results which have considerable variation: 80(30) keV [18], 120(20) keV [19], 140(40) keV [20], and 140(30) keV (determined from the study of Ref. [21] and given in Ref. [22]). This wide variation in and of itself motivates the reexamination of the width of this state that the present work provides.

It is perhaps also worth pointing out that the next proton-capture reaction in the rap-II sequence is ^{12}N$(p,\gamma)^{13}$O. Again, direct capture to the ground state and resonance capture can contribute [3,7,23]. This provides additional motivation to gain a more complete understanding of the low-lying structure of ^{13}O.

In this work, we report on some new level information for ^{12}N and ^{13}O excited states obtained from an experiment with a ^{13}O beam. The results of this experiment concerning the multiple proton decay of both the ground state of ^{12}O and its isobaric analog state in ^{12}N have already been published [24]. Some details of the experiment not mentioned below can be found there. The results of the present work are summarized in Table I and in the level scheme of Fig. 1. The remainder of the paper is organized as follows. The experiment is described in Sec. II and the properties of the second excited state of ^{12}N is discussed in Sec. III. The properties of the newly found states of ^{13}O and a comparison to, and insight gained from, calculations of the continuum structure of ^{13}O are presented in Secs. IV and V, respectively. Section VI presents the theory for the radiative capture reaction ^{11}C$(p,\gamma)^{12}$N. While the theory is identical to that used in Ref. [14], in the present work, the theory is more fully presented and in Sec. VII employed with the new width of the second excited state of ^{12}N. The work concludes in Sec. VIII with a short summary of results.

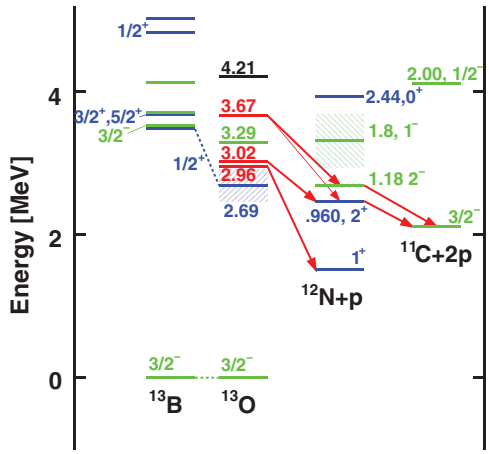

FIG. 1. (Color online) The level diagrams of ^{13}O and ^{12}N showing the levels discussed in this work and the observed proton decay branches. The ^{13}O levels can be compared to those for the mirror nucleus ^{13}B. When known, the negative parity states are shown in green, positive parity in blue. The ^{13}O levels found in this work are in red.

II. EXPERIMENTAL METHOD

At the Texas A&M University cyclotron facility, a primary beam of $E/A = 38$ MeV ^{14}N of intensity 80 pnA was extracted from the K500 cyclotron. This beam impinged on a hydrogen gas cell held at a pressure of 2.5 atmospheres at liquid nitrogen temperature. A secondary beam of 2000–4000 s^{-1} $E/A = 30.3$ MeV ^{13}O, separated from the other reaction products using the MARS spectrometer [25,26], impinged on a 45.6-mg/cm^2 target of ^{9}Be.

Particles of interest were detected in a multihit $\Delta E - E$ telescope located at 0°, 18 cm downstream of the target. The ΔE element consisted of a large-area double-side Si strip detector which also provided the angular measurements. This 300-μm Si detector had dimensions of 10 cm × 10 cm with 128 strips on both the front and back sides. Behind this was placed a 32-element array of 10-cm-thick CsI(Tl) scintillator E detectors to stop the particles. These detectors were arranged in a 6 × 6 array with the corner locations vacant. Energy calibrations of the Si strips were obtained from ^{228}Th and ^{241}Am α-particle sources. The particle-dependent light output of the CsI(Tl) detectors were calibrated using cocktail beams including p, ^{10}C, and ^{12}C particles with two energies each. The calibrations for ^{11}C were interpolated from the ^{10}C and ^{12}C results.

The experimental detection efficiency and resolution was obtained from Monte Carlo simulations incorporating the detector's angular and energy resolutions and most importantly the small-angle scattering [27] and the differential velocity loss of the protons and C fragments in leaving the target [28]. See Ref. [24] for more detail.

III. SECOND EXCITED STATE OF ^{12}N

All ^{12}N excited states are above the proton separation energy and thus most excited states are expected to have significant proton decay strength. The first excited state at $E^* = 0.960$ MeV [17] is strongly populated in neutron knockout reactions and was presented in Ref. [24]. In Fig. 2, the excitation-energy spectra from a selection of the detected $p+{}^{11}$C events is shown for the region around this strong peak at $E^* = 0.960$ MeV. In addition to this peak, a second much smaller peak at ∼1.2 MeV is clearly visible corresponding to the second excited state.

Two-body decays can be separated into transverse ($|\cos\theta_d| < 0.5$) and longitudinal ($|\cos\theta_d| > 0.5$) where θ_d is the angle between the reconstructed p-^{11}C relative velocity and their center-of-mass velocity vector. For transverse decays, the

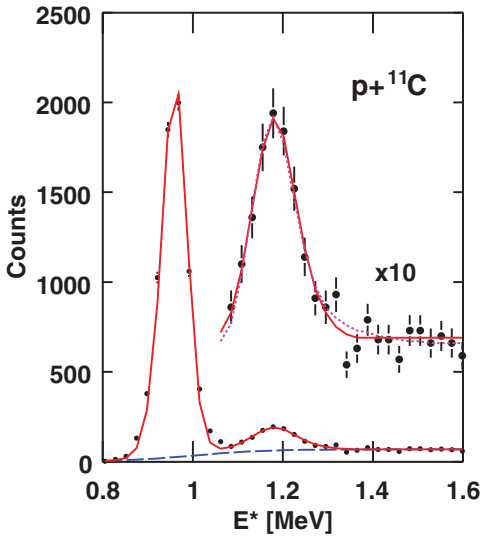

FIG. 2. (Color online) The ^{12}N excitation-energy spectra deduced with the invariant-mass method for detected $p + {}^{11}$C events associated with transverse decay. The higher-energy part of the spectrum is shown scaled by a factor of 10 to clearly show the fits to the second excited state. The solid curves show joint fits to the two peaks with the dashed curve indicating the fitted background. For the solid curve, the line shape of the second excited state was assumed to have a Breit-Wigner form. The dotted curve shows the equivalent result when an R-matrix line shape was assumed. The experimental and simulated spectra were binned in the same manner.

invariant mass resolution is largely independent of the energy calibrations of the CsI(Tl) detectors but very sensitive to the angular calibrations and vise versa for the longitudinal decays. In addition the Monte Carlo simulations indicate that the excitation-energy resolution for transverse decays are 1.8 times smaller than for the longitudinal decays. It is thus advantageous when determining a peak's centroid and width to focus on the transverse distribution which is shown in Fig. 2.

The solid curve shows Monte Carlo simulations of the first and second excited states with the addition of a smooth fitted background (dashed curve). These simulations included the resolution of the detection apparatus. The width of the first excited state is listed in ENSDF as $\Gamma < 20$ keV [17]. Even the upper limit of this width is well below our experimental resolution and thus the width of this intense peak in Fig. 2 comes almost entirely from the experimental resolution. The simulation reproduces the experimental width and centroid of this state exceedingly well.

The full width at half maximum (FWHM) of the peak associated with the second excited state is 106 keV which can be compared to the value of 73 keV for the first excited state that, as mentioned above, is almost entirely instrumental in origin. Moreover, our simulations suggest that the experimental resolution for the second excited state should be even larger than 73 keV, so the intrinsic width of this state should be significantly reduced from this 106-keV value. However, even without removing the experimental resolution, this FWHM is just within the uncertainty for the listed ENSDF value of the intrinsic width [$\Gamma = 118(14)$ keV [17]]. However, as already stated in Sec. I, there are a wide range of experimental values measured for this width and as it has astrophysical interest, it is useful to extract a value from the present work.

The curves in Fig. 2 were obtained from fits where both the centroid and intrinsic width of this state were varied and the instrumental resolution added via the Monte Carlo simulation. The solid curve shows a fit using the Breit-Wigner line shape where the fitted values are $E^* = 1.181(7)$ MeV and $\Gamma = 59(20)$ keV and the errors quoted are purely statistical. The dotted curve shows the results using the R-matrix line shape for an isolated resonance [29]:

$$N_{12}(E) \propto \frac{\Gamma(E)}{[E - E_R - \Delta(E)]^2 + [\Gamma(E)/2]^2}, \quad (1)$$

$$\Gamma(E) = 2\gamma^2 P_\ell(E), \quad (2)$$

$$\Delta(E) = -\gamma^2[S_\ell(E) - S_\ell(E_R)], \quad (3)$$

where E is the decay energy ($E = E^*$-0.601 MeV), $P_\ell(E)$, and $S_\ell(E)$ are the barrier penetration factor and shift functions;

$$P_\ell(E) = \frac{k\, r_0}{F_\ell^2(kr_0) + G_\ell^2(kr_0)}, \quad (4)$$

$$S_\ell(E) = \frac{F'_\ell(kr_0)F_\ell(kr_0) + G'_\ell(kr_0)G_\ell(kr_0)}{F_\ell(kr_0)^2 + G_\ell(kr_0)^2}, \quad (5)$$

where $F_\ell(kr)$ and $G_\ell(kr)$ are the regular and irregular Coulomb wave functions and k is the wave number. These were calculated with a channel radius of $r_0 = 1.45$ fm $(A_1^{1/3} + A_2^{1/3})$ and $\ell = 0$.

The fit gives a reduced width of $\gamma^2 = 0.65(35)$ MeV and a resonant energy of $E_R = 0.576$ MeV ($E^* = 1.176(7)$ MeV). The observed width is $\Gamma_{\rm obs} = \Gamma(E_R)/(1 - \Delta'(E_R))$ [29] which has a value of 51(20) keV. Both the centroid and width are consistent with the results of the Breit-Wigner fit. With a systematic uncertainty of 10 keV [24], the centroids are also consistent with the ENSDF value of 1.191(8) MeV. As already suggested, the width is considerably narrower than the listed ENSDF value of 118(14) keV. Our new value of the width is, however, consistent with the 80(30)-keV measurement of Ref. [18], but inconsistent with the other measured values.

It is perhaps worth pointing out that as the energy of the excited states in ^{12}N were determined assuming that the ^{11}C fragment was produced in its ground state. However, as ^{11}C has a number of particle-bound states, it is in principle possible that the peak discussed in this section, the second peak in Fig. 2, results from the decay of a higher lying level where we have not accounted for an undetected gamma ray. However, this seems highly unlikely as the energy of this peak is, within our small uncertainty, exactly the energy expected for the second excited state.

IV. ^{13}O STATES

Three new levels, excited by inelastic scattering, were found in ^{13}O. The excitation-energy spectra, deduced by the invariant-mass method from detected $p + {}^{12}$N and $2p + {}^{11}$C events are shown in Figs. 3(a) and 3(b), respectively. To improve resolution, only the distribution for the transverse decays is shown in Fig. 3(a). For the three-body exit channels, the fraction of the events where all fragments are emitted

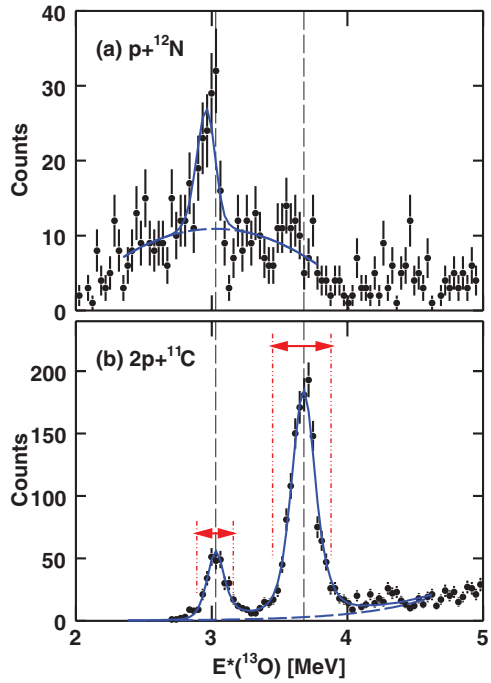

FIG. 3. (Color online) The ^{13}O excitation-energy spectra deduced with the invariant-mass method for detected (a) $p + {}^{12}$N and (b) $2p + {}^{11}$C events. The solid curves shown are fits to the peaks where the peak shape is taken from simulations including the experimental response and with $\Gamma = 0$. The dashed curves are smooth backgrounds fitted to the data. The excitation-energy gates for further analysis of the two peaks in (b) are indicated.

transversely to the parent velocity vector is quite small, so the displayed spectrum, Fig. 3(b), uses the full statistics.

The states corresponding to the observed peaks are relatively narrow as indicated by the fits shown by the solid curves that are from the Monte Carlo simulations which include the effects of the detector resolution, but with no intrinsic width ($\Gamma = 0$). Thus for all three peaks, the experimental width is consistent with the experimental resolution and we estimate that the intrinsic widths are less than $\Gamma = 50$ keV.

The fitted peak energies correspond to excitation energies of 2.956(10) MeV for the peak in the $p + {}^{12}$N channel and 3.025(6) MeV and 3.669(3) MeV for the two peaks in the $2p + {}^{11}$C channel. The errors quoted here are purely statistical and we again estimate a further 10-keV systematic error [24]. The 2.956 MeV ($p + {}^{12}$N) and 3.025 MeV ($2p + {}^{11}$C) peaks have very similar energies and one may wonder if they are just two branches of the same level. The dashed, vertical lines in Figs. 3(a) and 3(b) help one compare the peak locations in the two spectra. The fitted peak values are separated by 69 keV, which is many times the uncertainties in the resonance energies and larger than our limit of 50 keV for the intrinsic widths, and so the most likely interpretation is that these are two distinct levels. However, if these were two branches of the same state, it would decay 29(8)% and 71(8)% to the ground and first excited states of ^{12}N, respectively.

For the $2p + {}^{11}$C exit channel, one can consider both a direct three-body decay or a sequential decay process passing through ^{12}N intermediates states. Information on the decay path can be gleaned from the momentum correlations between the detected fragments. In three-body decay, ignoring spin degrees of freedom, these can be completely described by two-dimensional distributions [30] and the most common representations are in terms of the hyperspherical Jacobi coordinates. The two commonly employed and equivalent representations are called the Jacobi T and Y systems [30]. In this work we will focus only on the Y representation where the correlations are described by the parameters E_x/E_T and $\cos(\theta_k)$. Labeling the protons as p_1 and p_2, then E_x is the relative kinetic energy between p_1 and the core or ultimate residue (^{11}C), E_T is the total decay kinetic energy, and θ_k is the angle between the p_1-core relative momentum and the momentum of p_2 in the decay center-of-mass frame. If both protons are emitted in the same direction, then $\theta_k = 0^\circ$. The experimental Jacobi Y correlation plots are shown in Figs. 4(a) and 4(b) for the 3.02-MeV and 3.67-MeV states, respectively. For each detected event, these distributions were incremented twice, once for each of the two protons given the p_1 label.

Both correlations plots show the presence of two separate bands which is a clear signature of sequential decay. This can be contrasted with the correlations expected for three-body decay in light nuclei where one continuous distribution is observed [30,31]. For both excited states, only one of the two bands has a constant value of E_x/E_T, i.e., independent of the angular coordinate. This is the left-most band in both Figs. 4(a) and 4(b) with E_x/E_T ~0.36. This band corresponds to the case where the proton labeled p_1 is the second proton emitted, i.e., the proton produced by the sequential decay of the ^{12}N intermediate state to the ^{11}C core. The quantity E_x in this case is just the decay energy of the intermediate state which should be independent of the angular coordinate. When the first emitted proton is labeled as p_1, then the relative energy between it and the core depends on the recoil momentum imparted by the second emitted proton. With the protons labeled in this fashion, a second band is generated that should show a dependence on the relative recoil direction θ_k. These are the right-most bands in Figs. 4(a) and 4(b). The association of these bands are confirmed by the Monte Carlo simulations shown in Fig. 4(c) of the decay of the level at $E^* = 3.67$ MeV, see Fig. 4, which used the branching ratios given in Table I.

The excitation energy of the intermediate state can readily be determined by projecting on the E_x axis and adding the decay Q value. The ^{12}N excitation-energy spectra obtained in this manner are shown for the 3.02-MeV and 3.67-MeV ^{13}O states in Figs. 5(a) and 5(b), respectively. For reference, the thin-vertical-dotted lines show the location of the 0.960-MeV and 1.179-MeV ^{12}N levels observed in the $p + {}^{11}$C exit channel (Sec. III).

Both spectra have two prominent peaks, a lower-energy narrow peak corresponding to the bands in Figs. 4(a) and 4(b) with constant E_x/E_T and a broader higher-energy peak corresponding to the band with the large θ_k dependence. As indicated before, only the lower-energy narrow peak is associated with a ^{12}N excited state. In Fig. 5(a), this peak is consistent with the 0.960-MeV state of ^{12}N. The curve in Fig. 5(a) shows the results of a Monte Carlo simulation of a sequential decay through this narrow state ($\Gamma < 10$ keV) including the detector response and resolution. In this simulation, the width of the

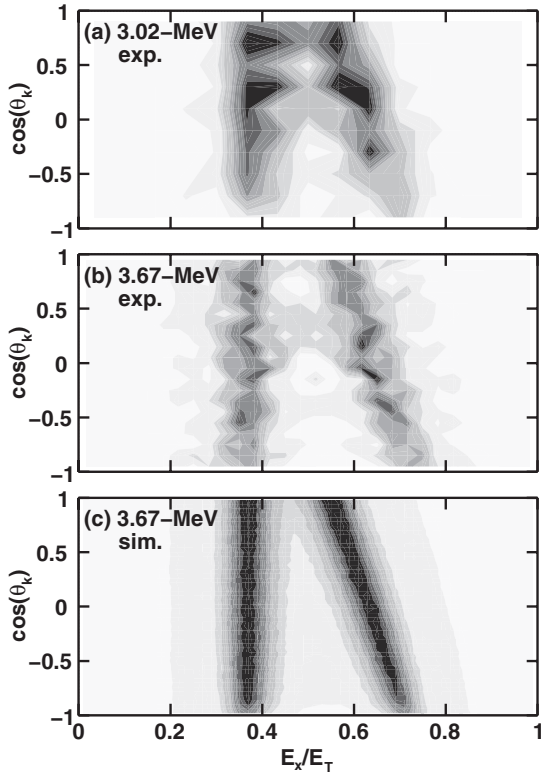

FIG. 4. Population of the decay phase space, as described by the Jacobi Y coordinates, for $2p+{}^{11}$C channels. Shown are the experimental distributions for (a) 3.02-MeV and (b) 3.67-MeV ^{13}O states and (c) a simulation of the 3.67-MeV ^{13}O state.

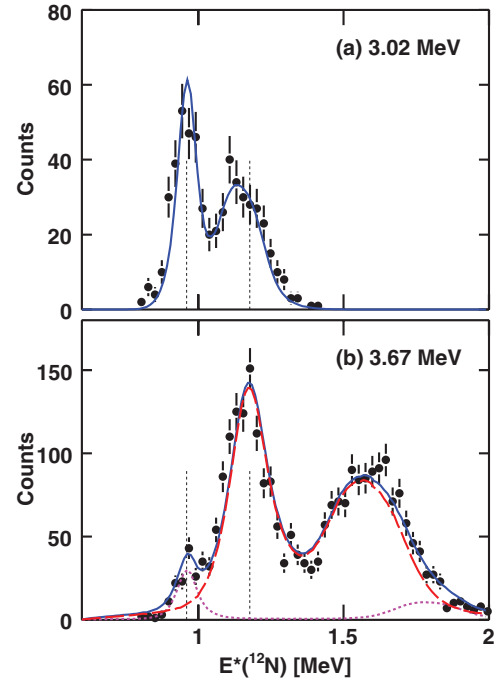

FIG. 5. (Color online) Distribution of ^{12}N excitation energy determined from each of the two $p+{}^{11}$C combinations associated with detected $2p+{}^{11}$C events. Results are shown for (a) 3.02-MeV and (b) 3.67-MeV states in ^{13}O [gates shown in Fig. 3(b)]. Experimental results are indicated by the data points and the solid curves show the results of sequential-decay simulations. In (b), the dotted and dashed curves indicate the fitted contributions from sequential decays to the first and second excited states of ^{12}N, respectively.

lower peak is entire due to the detector resolution and the simulation reproduces the data quite well confirming that this is the dominant decay branch. We cannot rule out a small branch to the 1.179-MeV state as the second peak in Fig. 5(a) encompasses the energy of this state. However, significant branch of this type would alter the two-band pattern observed in Fig. 4(a).

For the decay of the 3.67-MeV ^{13}O state [Fig. 5(b)], the prominent low-energy peak is located very close to the known 1.179-MeV state in ^{12}N. In addition to the two prominent peaks, we also see a small low-energy shoulder at the energy corresponding to the 0.960-MeV state in ^{12}N. Thus the experimental distribution suggests a strong decay branch to the 1.179-MeV second-excited state plus a weak decay branch to the 0.960 first-excited state. To quantity this, we have simulated both of these decays and the solid curve in Fig. 5(b) shows the fitted distribution including the effects of the detector response and resolution. The contribution from the sequential decay to the 0.960-MeV state is shown as the dotted curve in Fig. 5(b). The dashed curve indicates the contribution from the 1.179-MeV state which has a significant width and so one must fold in the interplay of its line shape [Eq. (1)] with the barrier penetration factor of the first proton. This was achieved with the R-matrix formalism [29] where the distribution of E_x is

$$N_{13}(E_x) \propto P_{\ell_1}(E_T - E_x)N_{12}(E_x). \quad (6)$$

As the spin of the 3.67-MeV state is unknown, the value of ℓ_1, the orbital angular momentum removed by the first step, is also unknown. Note there are no angular correlations between the two decay steps as the second step is $\ell_2 = 0$. The fit shown in Fig. 5(b) was obtained with $\ell_1 = 1$. For parameters associated with the line shape of the ^{12}N state $N_{12}(E_x)$ [Eq. (1)], the resonance energy was fixed to its value of $E_r = 1.176$ MeV from the R-matrix fit (Sec. III) and the reduced width γ^2 was taken as a fit parameter as well as the branching ratio $\Gamma_1/\Gamma_{\rm tot}$ to the first excited state. The fitted values are $\gamma^2 = 0.91(14)$ and $\Gamma_1/\Gamma_{\rm tot} = 10(2)\%$ and the corresponding observed width $\Gamma_{\rm obs} = 69(7)$ keV is consistent with the value of 51(20) keV extracted from the $p+{}^{11}$C data in Sec. III. However, the fitted observed width is dependent on the assumed value of ℓ_1. For $\ell_1 = 0$ we obtain $\Gamma_{\rm obs} = 58(8)$ keV, again consistent, but for $\ell_2 = 2$ we find $\Gamma_{\rm obs} = 82(6)$ keV which is starting to be outside the statistical uncertainty. This suggests that ℓ_1 is probably 0 or 1. Note that even with an unrealistic value of $\ell_1 = 4$, we obtain $\Gamma_{\rm obs} = 90(10)$ keV which is still below the ENSDF value of 118(14) keV. This confirms that these $2p+{}^{11}$C data cannot be reconciled with the listed value of the width of the 2^- state in ^{12}N.

It is again perhaps worth pointing out the potential consequences of our assignments based on the assumption of the absence of producing particle-bound excited states. This issue is irrelevant for the state at 2.956 MeV as ^{12}N has no bound excited states. Nor is this assumption of relevance for the

nearby and presumably different state at 3.025 MeV as the intermediate in its decay (the 0.960-MeV state in ^{12}N) is known to decay to the ground state of ^{11}C. It is, however, in principle, possible that the state we have labeled at 3.669 MeV is really at higher energy. However, this interpretation is problematic as the weak low-energy shoulder seen in Fig. 5(b) could not be a weak decay branch to the first excited state of ^{12}N which is known to decay to the ground state of ^{11}C. This logic would then still imply a level at 3.669 MeV, but not with the strong decay property we ascribe to it, as well as another level at a higher energy. This hypothetical higher-energy state would decay to a level in ^{12}N with an energy above the $J^\pi = 2^-$ equal to the missed energy of the excited (but bound) ^{11}C residue. While possible, this is unlikely.

V. DISCUSSION

Figure 1 displays the level schemes of both ^{13}O and its mirror ^{13}B. The latter has benefited from a recent HELIOS experiment [32]. The $1/2^+$ first excited state is ∼790 keV lower in excitation energy in ^{13}O. This was interpreted as a possible Thomas-Ehrman effect associated with strength in the loosely bound $1s_{1/2}$ level [3]. We have found evidence for at least one and perhaps two more levels in ^{13}O well below the first excited state in ^{13}B. This new level or levels (with centroids at 2.96 and 3.02 MeV) are then also likely associated with significant Thomas-Ehrman shifts and therefore s-wave strength.

Preliminary calculations have been done to gain some insight into the low-lying level structure of these $A = 13$ nuclei with particular focus on the effect of the continuum. We employed the recently introduced unified approach which melds the no-core shell model (NCSM) to the resonating-group method (RGM). The latter, a scattering technique, enforces the proper Whittaker and/or Coulomb function asymptotic form for continuum states. This unified approach is called the no-core shell model with continuum (NCSMC) [33,34]. These calculations, which use a soft similarity renormalization evolved (SRG) [35–37] chiral nucleon-nucleon interation [38] and do not include three-nucleon interactions (an omission that leads to a general overbinding of the nuclei considered here), suggest that physical states with considerable $1s_{1/2}$ spectroscopic strength can be found with $J^\pi = 1/2^+$ and $3/2^+$ built on the $J^\pi = 1^+$ ground state of ^{12}N. A $J^\pi = 5/2^+$ state is found built on the ^{12}N first excited state ($J^\pi = 2^+$) and an s-wave proton. Similarly these calculations also indicate that there is a higher lying $J^\pi = 3/2^-$ state (the third of this J^π) built on the ^{12}N $J^\pi = 2^-$ with mostly s but some d-wave character.

The first excited state at $E^* = 2.69$ MeV has previously been assigned as $J^\pi = 1/2^+$. If the two newly found levels near 3 MeV are really distinct, the lower of the two at $E^* = 2.96$ MeV (which decays to $^{12}\mathrm{N}_{g.s.}$) is then likely the $J^\pi = 3/2^+$ while the level at $E^* = 3.02$ MeV (which decays to the first excited state of ^{12}N with $J^\pi = 2^+$) is likely $J^\pi = 5/2^+$. The s-wave and unbound character of all these physical states allows them to be at lower excitation energy than their analogs in ^{13}B. Making these tentative assignments, the $J^\pi = 1/2^+$, $3/2^+$, and $5/2^+$ levels are downshifted by 0.79, 0.72, and 0.69 MeV in ^{13}O as compared to ^{13}B. On the other hand, if the structures found at $E^* = 2.96$ and 3.02 MeV are two branches of the same state the fact that most of the decay is going to the excited $J^\pi = 2^+$ state in ^{12}N, rather than the ground state with almost three times the decay energy, would suggest that this state has a somewhat simple structure of a predominately s-wave proton coupled to a $J^\pi = 2^+$ ^{12}N core.

The previously known state at $E^* = 3.29$ MeV could be the mirror of the $J^\pi = 3/2^-_2$ second excited state in ^{13}B for which a ν2p2h configuration was inferred [4]. If this were the case, the level in ^{13}O would be downshifted by 240 keV, 1/2 to 1/3 of the downshift of the levels with the major single nucleon s-wave character. Finally, the strong decay branch of the state found at $E^* = 3.67$ MeV is consistent with the higher lying $J^\pi = 3/2^-$ state predicted by the NCSMC calculations. The present calculations do not provide any insight into the weak (10%) decay branch to the $J^\pi = 2^+$ state of ^{12}N.

All of the decays discussed above, aside from the weak branch just mentioned, can proceed by s-wave proton emission. The calculations, and the tentative assignments made above, will be revisited in future work that includes three-nucleon interactions [39]. It might be appropriate at that time to revisit the $^{12}\mathrm{N}(p,\gamma)^{13}\mathrm{O}$ reaction [23].

VI. *R*-MATRIX ANALYSIS FOR RADIATIVE CAPTURE

Let us consider the $a + A \to B + \gamma$ radiative-capture process. The R-matrix radiative-capture cross section to a state in nucleus B with a given spin J_f is given by [40]

$$\sigma_{J_f}(E) = \frac{\pi}{k^2} \sum_{J_i I l_i} \frac{\hat{J}_i}{\hat{J}_a \hat{J}_A} |U_{I l_f l_i J_f J_i}(E)|^2. \tag{7}$$

Here, $\hat{J} = 2J + 1$, J_i is the total angular momentum of the colliding nuclei a and A in the initial state, J_a and J_A are their spins, I and l_i are their channel spin and orbital angular momentum, and k is the relative $a - A$ momentum related to their relative kinetic energy E as $k = \sqrt{2\,\mu_{aA}\,E}$, where μ_{aA} is the reduced mass. In what follows, we use the system of units in which $\hbar = c = 1$. $U_{I l_f l_i J_f J_i}(E)$ is the transition amplitude from the initial continuum state (J_i, I, l_i) to the final bound state (J_f, I, l_f). It is given by the sum of resonant $U^R_{I l_f l_i J_f J_i}(E)$ and nonresonant $U^{\mathrm{NR}}_{I l_f l_i J_f J_i}(E)$ transition amplitudes:

$$U_{I l_f l_i J_f J_i}(E) = U^R_{I l_f l_i J_f J_i}(E) + U^{\mathrm{NR}}_{I l_f l_i J_f J_i}(E). \tag{8}$$

The resonant amplitude can have contributions by multipole resonances and the resonant and nonresonant amplitudes with the same quantum numbers do interfere. In the one-level, one-channel R-matrix approach, the resonant amplitude $U^R_{I l_f l_i J_f J_i}$ for capture into a resonance with energy E_R and spin J_i, and subsequent decay into the bound state with spin J_f, is given by

$$U^R_{I l_f l_i J_f J_i} = -i e^{i(\omega_{l_i} - \phi_{l_i})} \frac{\left[\Gamma^{J_i}_{aA\,I l_i}(E)\right]^{1/2} \left[\Gamma^{J_i}_{\gamma J_f}(E)\right]^{1/2}}{E - E_R + i\frac{\Gamma^{J_i}(E)}{2}}. \tag{9}$$

The phase factor ϕ_{l_i} is the solid-sphere scattering phase shift for the l_ith partial wave and ω_{l_i} is given by

$$\omega_{l_i} = \sum_{n=1}^{l_i} \tan^{-1}\left(\frac{\eta_i}{n}\right), \tag{10}$$

where $\eta_i = Z_a\, Z_A\, \mu_{aA}/k$ is the Coulomb parameter in the initial state, and Z_j is the charge of the particle j. $[\Gamma^{J_i}_{aA\,Il_i}(E)]^{1/2}$ is real and its square, $\Gamma^{J_i}_{aA\,Il_i}(E)$, is the observable partial width of the resonance in the channel $a + A$ with the given set of quantum numbers, and $\Gamma^{J_i}(E)$ is the total resonance width which we approximate as $\Gamma^{J_i}(E) \approx \sum_I \Gamma^{J_i}_{aAIl_i}(E)$; $[\Gamma^{J_i}_{\gamma J_f}(E)]^{1/2}$ is complex and its modulus square is the observable radiative width:

$$\Gamma^{J_i}_{\gamma\,J_f}(E) = \left|\left[\Gamma^{J_i}_{\gamma\,J_f}(E)\right]^{1/2}\right|^2. \tag{11}$$

The energy dependence of the partial and radiative widths are given by

$$\Gamma^{J_i}_{aA\,Il_i}(E) = \frac{P_{l_i}(E)}{P_{l_i}(E_R)}\,\Gamma^{J_i}_{aA\,Il_i}(E_R), \tag{12}$$

and

$$\Gamma^{J_i}_{\gamma\,J_f}(E) = \left(\frac{E+\varepsilon_f}{E_R+\varepsilon_f}\right)^{2L+1}\Gamma^{J_i}_{\gamma\,J_f}(E_R), \tag{13}$$

respectively. Here, $\Gamma^{J_i}_{aAIl_i}(E_R)$ and $\Gamma^{J_i}_{\gamma\,J_f}(E_R)$ are the experimental partial and radiative resonance widths, ε_f is the binding energy of the bound state $B = (aA)$ for the virtual decay $B \to a + A$, and L is the multipolarity of the gamma quanta emitted during the transition.

In a strict R-matrix approach, the radiative width $\Gamma^{J_i}_{\gamma J_f}(E)$ can be expressed in terms of the real internal $[\Gamma^{J_i}_{\gamma\,(\mathrm{int})\,J_f}(E)]^{1/2}$ and complex external $[\Gamma^{J_i}_{\gamma\,(\mathrm{ch})J_f}(E)]^{1/2} = \mathrm{Re}[\Gamma^{J_i}_{\gamma(\mathrm{ch})J_f}(E)]^{1/2} + i\,\mathrm{Im}[\Gamma^{J_i}_{\gamma(\mathrm{ch})J_f}(E)]^{1/2}$ channel radiative-width amplitudes [40,41]:

$$\begin{aligned}\Gamma^{J_i}_{\gamma J_f}(E) &= \left|-\left[\Gamma^{J_i}_{\gamma\,(\mathrm{int})\,J_f}(E)\right]^{1/2} + \left[\Gamma^{J_i}_{\gamma\,(\mathrm{ch})\,J_f}(E)\right]^{1/2}\right|^2 \\ &= \left(\mathrm{Re}\left[\Gamma^{J_i}_{\gamma\,(\mathrm{ch})\,J_f}(E)\right]^{1/2} - \left[\Gamma^{J_i}_{\gamma\,(\mathrm{int})\,J_f}(E)\right]^{1/2}\right)^2 \\ &\quad + \left(\mathrm{Im}\left[\Gamma^{J_i}_{\gamma\,(\mathrm{ch})\,J_f}(E)\right]^{1/2}\right)^2.\end{aligned} \tag{14}$$

The channel radiative-width amplitude is given by [40]

$$\begin{aligned}[\Gamma^{J_i}_{\gamma\,(\mathrm{ch})\,J_f}(E)]^{1/2} &= \sqrt{2}\,i^{l_i+L-l_f+1}\,\frac{1}{k}\,{\mu_{aA}}^{L+1/2}\left(\frac{Z_a\,e}{m_a^L} + (-1)^L\,\frac{Z_A\,e}{m_A^L}\right)\sqrt{\frac{(L+1)\hat{L}}{L}}\,\frac{1}{\hat{L}!!} \\ &\quad\times (k_\gamma\, r_0)^{L+1/2}\, C_{J_f I l_f}\sqrt{\Gamma^{J_i}_{aA\,Il_i}(E_R)}\,\sqrt{P_{l_i}(E)}\,([F_{l_i}(kr_0)]^2 \\ &\quad + [G_{l_i}(kr_0)]^2)\, W_{-\eta_{aA},\,l_f+1/2}(2\,\kappa\, r_0)\,(l_i 0\, L0|l_f 0)\,U(L\,l_f\,J_i\,I;\,l_i\,J_f)\,J_L(l_f, l_i),\end{aligned} \tag{15}$$

$$J_L(l_f, l_i) = J_L^{''}(l_f, l_i) + i\,\frac{F_{l_i}(kr_0)\,G_{l_i}(kr_0)}{F_{l_i}^2(kr_0) + G_{l_i}^2(kr_0)}\,J_L^{'}(l_f, l_i), \tag{16}$$

$$J_L^{''}(l_f, l_i) = \frac{1}{r_0^{L+1}}\int_{r_0}^{\infty} dr\, r^L\,\frac{W_{-\eta_{aA},\,l_f+1/2}(2\,\kappa\, r)}{W_{-\eta_{aA},\,l_f+1/2}(2\,\kappa\, r_0)}\,\frac{F_{l_i}(kr)\,F_{l_i}(kr_0) + G_{l_i}(kr)\,G_{l_i}(kr_0)}{F_{l_i}^2(kr_0) + G_{l_i}^2(kr_0)}, \tag{17}$$

$$J_L^{'}(l_f, l_i) = \frac{1}{r_0^{L+1}}\int_{r_0}^{\infty} dr\, r^L\,\frac{W_{-\eta_{aA},\,l_f+1/2}(2\,\kappa\, r)}{W_{-\eta_{aA},\,l_f+1/2}(2\,\kappa\, r_0)}\left[\frac{F_{l_i}(kr)}{F_{l_i}(kr_0)} - \frac{G_{l_i}(kr)}{G_{l_i}(kr_0)}\right]. \tag{18}$$

Here, $C_{J_f I l_f}$ is the asymptotic normalization coefficient (ANC) for the virtual decay $B \to a + A$, $W_{-\eta_{aA},\,l_f+1/2}(2\,\kappa\, r)$ is the Whittaker function, η_{aA} is the Coulomb parameter of the bound state $B = (aA)$, r_0 is the channel radius, which determines the border dividing the internal and external regions, $\kappa = \sqrt{2\,\mu_{aA}\,\varepsilon_f}$, $(l_i 0\, L0|l_f 0)$ is the Clebsch-Gordan coefficient, and $U(L\,l_f\,J_i\,I;\,l_i\,J_f)$ is a 6j symbol. In addition, $k_\gamma = E + \varepsilon_f$ is the momentum of the emitted photon.

Assuming that the experimental radiative width $\Gamma^{J_i}_{\gamma J_f}(E_R)$, the ANC of the bound state, and the resonance width $\Gamma^{J_i}_{aA\,Il_i}(E_R)$ are known we can determine

$$\Gamma^{J_i}_{\gamma\,(\mathrm{int})\,\mathrm{J_f}}(E) = \left[\,\mathrm{Re}\left[\Gamma^{J_i}_{\gamma\,(\mathrm{ch})\,\mathrm{J_f}}(E)\right]^{1/2} \pm \sqrt{\Gamma^{J_i}_{\gamma J_f}(E) - \left(\mathrm{Im}\left[\Gamma^{J_i}_{\gamma\,(\mathrm{int})\,\mathrm{J_f}}(E)\right]^{1/2}\right)^2}\,\right]^2. \tag{19}$$

In the R-matrix method, the internal nonresonant amplitude is absorbed into the internal resonance term, so that the nonresonant capture amplitude is entirely contributed by the channel (external) term:

$$\begin{aligned}U^{\mathrm{NR}}_{I\,l_f\,l_i\,J_f\,J_i}(E) &= -i(2)^{3/2}\,i^{l_i+L-l_f+1}\,e^{i(\omega_{l_i}-\phi_{l_i})}\,\frac{1}{k}\,{\mu_{aA}}^{L+1/2}\left(\frac{Z_a\,e}{m_a^L} + (-1)^L\,\frac{Z_A\,e}{m_A^L}\right)\sqrt{\frac{(L+1)\hat{L}}{L}}\,\frac{1}{\hat{L}!!}\,(k_\gamma\, r_0)^{L+1/2} \\ &\quad\times C_{J_f I l_f}\,F_{l_i}(kr_0)\,G_{l_i}(kr_0)\,W_{-\eta_{aA},\,l_f+1/2}(2\,\kappa\, r_0)\sqrt{P_{l_i}(E)}\,(l_i 0\, L0|l_f 0)\,U(L\,l_f\,J_i\,I;\,l_i\,J_f)\,J_L^{'}(l_i\,l_f).\end{aligned} \tag{20}$$

The sum of the interfering resonant and nonresonant amplitudes is given by [40]

$$U^{R}_{I l_f l_i J_f J_i}(E) = U^{R(\mathrm{int})}_{I l_f l_i J_f J_i}(E) + U^{R(\mathrm{ch})}_{I l_f l_i J_f J_i}(E) + U^{\mathrm{NR}}_{I l_f l_i J_f J_i}(E). \quad (21)$$

The internal and external resonant radiative-capture amplitudes, describing the capture of the incident particle a by A into the resonant state with subsequent decay to the bound state at distances $r \leqslant r_0$ and $r > r_0$, correspondingly, are given by

$$U^{R(\mathrm{int})}_{I l_f l_i J_f J_i}(E) = i e^{i(\omega_{l_i} - \phi_{l_i})} \frac{\left[\Gamma^{J_i}_{aA\, I l_i}(E)\right]^{1/2}\left[\Gamma^{J_i}_{\gamma\,(\mathrm{int})\, J_f}(E)\right]^{1/2}}{E_R - E - i\frac{\Gamma^{J_i}(E)}{2}}, \quad (22)$$

and

$$U^{R(\mathrm{ch})}_{I l_f l_i J_f J_i}(E) = -i e^{i(\omega_{l_i} - \phi_{l_i})} \frac{\left[\Gamma^{J_i}_{aA\, I l_i}(E)\right]^{1/2}\left[\Gamma^{J_i}_{\gamma\,(ch)\, J_f}(E)\right]^{1/2}}{E_R - E - i\frac{\Gamma^{J_i}(E)}{2}}. \quad (23)$$

Note that the sign of the internal part is not known and can be determined only from the microscopic calculations.

VII. ASTROPHYSICAL APPLICATION

The $^{11}\mathrm{C}(p,\gamma)^{12}\mathrm{N}$ reaction may be an important branch point in bypassing the slow 3α process when producing CNO nuclei in very-low metallicity, massive stars [7]. The astrophysical factor for $^{11}\mathrm{C}(p,\gamma)^{12}\mathrm{N}$ was calculated in Ref. [14] and later on in Refs. [15,16].[1] This reaction at astrophysically relevant energies has contributions from the narrow first and broad second resonances in $^{12}\mathrm{N}$ and from direct capture to the ground state. The amplitude of the resonant capture through the second resonance and nonresonant capture amplitude at the channel spin $I = 2$ do interfere. The astrophysical factor was calculated in Ref. [14] using the measured ANC and the parameters of the first and second resonances. The contribution from the third resonance was found to be negligible. The cross section due to capture through the first resonance was estimated with the Breit-Wigner formula. In these calculations, the experimental proton widths were taken from Refs. [17,42]. Only an upper limit of 20 keV is available for the proton width of the first excited state. It was set to 5.5 keV, as suggested in Ref. [11], but the contribution from this narrow resonance over the region of interest depends only on the radiative width of the first resonance, which was set at 2.6 ± 0.4 meV [7,11]. Its uncertainty was assumed to be the same as that of the lifetime of the first excited state of $^{12}\mathrm{B}$, which is about 15%. The total width of the second resonance was taken to be 118 ± 14 keV [17] and the radiative width of this resonance $\Gamma_{\gamma 2} = 13 \pm 0.5$ meV [43]. The analysis done in Ref. [14] shows that only the ANC, the radiative width of the first resonance, and the total width of the second resonance are found to make significant contributions to the uncertainty of the astrophysical factor $S(E)$ for $E < 0.7$ MeV, (see Fig. 9 of Ref. [14]).

In this work a new value of the resonance width of the second resonance 51 ± 20 keV at the resonance energy $E_{R_2} = 576$ keV was extracted. Because this width is significantly smaller than the previously used one in [14–16], we recalculate the astrophysical factor for the $^{11}\mathrm{C}(p,\gamma)^{12}\mathrm{N}$ radiative capture. The change of the resonance width of the second resonance affects also the channel resonance amplitude [see Eq. (15)], and, correspondingly, the internal part of the radiative width of the second resonance.

The calculated $S(E)$ factor in the case under consideration is given by

$$S(E) = 5\pi(0.2118)^2 \frac{\hat{J}_i}{\hat{J}_A\,\hat{J}_a}\mu_{aA}(931.5)^2 e^{2\pi\eta_i}\left[\left|U^{R_1}_{I_1 l_f J_f J_i}(E)\right|^2 + \left|U^{R_2(\mathrm{int})}_{I_2 l_f J_f J_i}(E) + U^{R_2(\mathrm{ch})}_{I_2 l_f J_f J_i}(E) + U^{\mathrm{NR}}_{I_2 l_i J_f J_i}(E)\right|^2\right]\mathrm{keVb}. \quad (24)$$

Here, $J_A = 3/2$, $J_a = 1/2$, $I_1 = 1$, $I_2 = 2$, $l_i = 0$, $l_f = 1$, $J_f = 1$, $J_i = J_{R_1} = J_{R_2} = 2$, $l_1 = 1$, $l_2 = 0$, $L = 1$. In Eq. (24) μ_{aA} is expressed in MeV and the astrophysical factor $S(E)$ in keVb.

At the second resonance energy $E_{R_2} = 576$ keV, the calculated channel radiative width amplitude is

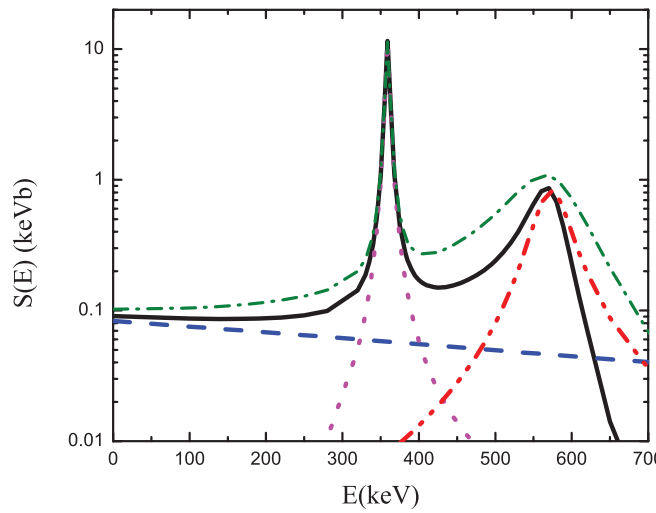

FIG. 6. (Color online) The $S(E)$ factor for $^{11}\mathrm{C}(p,\gamma)^{12}\mathrm{N}$. The black solid line is our updated total $S(E)$ factor calculated using a new determined width of 51 keV (the value extracted with the R-matrix analysis) for the second resonance. For comparison the green dashed-dotted line shows the $S(E)$ factor from [14] calculated using the 118 keV width of the second resonance. All other input parameters in the current and previous calculations in [14] are the same. The direct capture contribution is shown as the blue dashed line, the magenta dotted line is the first resonance contribution, and the red dashed-dotted-dotted line is the contribution from the second resonance.

[1]Note that the interference of the resonant and nonresonant terms used in [15] is not correct.

TABLE II. The low-energy astrophysical factors for $^{11}C + p \rightarrow {}^{12}N + \gamma$: energy in keV, present adopted astrophysical factor $S(E)$, and astrophysical factor from [14] in keVb.

E (keV)	Present $S(E)$ (keVb)	$S(E)$ from [14] (keVb)	E (keV)	Present $S(E)$ (keVb)	$S(E)$ from [14] (keVb)
10	0.090	0.102	455	0.162	0.342
100	0.087	0.103	465	0.172	0.373
140	0.087	0.107	475	0.185	0.412
170	0.086	0.111	485	0.203	0.459
190	0.087	0.114	495	0.226	0.516
220	0.088	0.120	500	0.240	0.548
250	0.092	0.129	510	0.277	0.623
280	0.099	0.143	530	0.401	0.812
320	0.143	0.199	550	0.654	1.013
330	0.187	0.248	560	0.816	1.073
340	0.318	0.383	570	0.865	1.072
350	1.065	1.135	580	0.679	0.999
359	11.56	11.637	589	0.438	0.885
368	1.09	1.168	598	0.259	0.750
375	0.446	0.530	600	0.230	0.720
382	0.279	0.368	610	0.126	0.575
390	0.207	0.303	620	0.071	0.450
400	0.171	0.275	650	0.014	0.213
410	0.156	0.270	695	0.003	0.077
420	0.151	0.275	705	0.003	0.062
430	0.150	0.288	715	0.004	0.051

$[\Gamma^{J_i}_{\gamma\,(\mathrm{ch})\,J_f}(E_{R_2})]^{1/2} = 0.00015392 + i0.0000273049\ \mathrm{MeV}^{1/2}$. From Eq. (19), we get two values of the internal radiative width; $\Gamma^{J_i(+)}_{\gamma\,(\mathrm{int})\,J_f}(E_{R_2}) = 70.02$ meV and $\Gamma^{J_i(-)}_{\gamma\,(\mathrm{int})\,J_f}(E_{R_2}) = 1.87$ meV. A simple single-particle estimation shows that $\Gamma^{J_i(+)}_{\gamma\,(\mathrm{int})\,J_f}(E_{R_2})$ is too high and we therefore adopt the smaller value of 1.87 meV. Also from these single-particle calculations, we find that in Eq. (21) we should choose the positive sign.

The calculated astrophysical $S(E)$ factor obtained from Eq. ((24)) is shown in Fig. 6 and compared with the result from Ref. [14]. Numerical values of both astrophysical factors are given in Table II. The total and fractional uncertainties in the astrophysical S factor were investigated in Ref. [14] by varying the ANC for ^{12}N, the radiative width of the first resonance and the total resonance width of the second resonance within their respective uncertainties. Owing to the new value of the resonance width of the second resonance, we show in Fig. 7 the recalculated total uncertainty of the $S(E)$ contributed by the 12% uncertainty of the ANC [14], 15% uncertainty of the radiative width of the first resonance, and by the 39% uncertainty of the second resonance width. Table III provides the updated reaction rates $N_A < \sigma v >$ with a comparison to those previously published [14]. At $T_9 = 0.2$ our updated reaction rate is only 26% lower than then the value obtained in Ref. [14] and this only slightly changes the temperature-density conditions at which the $^{11}C(p,\gamma)^{12}N$ reaction dominates (see Fig. 11 from [14]). The updated reaction rates (in cm^3 mole^{-1} s^{-1}) are well approximated for $T_9 \leqslant 1.3$ by

$$N_A\langle\sigma\, v\rangle = \frac{1.25598 \times 10^6}{T_9^{2/3}}\, e^{-\frac{13.6546}{T_9^{1/3}}}, \tag{25}$$

and for $T_9 > 1.3$ by

$$N_A\,\langle\sigma\, v\rangle = 1.75284 \times 10^{11}\omega\gamma\, T_9^{-3/2} e^{-4.1625/T_9} + 14.617 \times 10^9 \times T_9^{-2/3} e^{-13.6586\, T_9^{-1/3}} S(E_0) + 24.9731\, T_9^{-2/3}\, e^{(-13.6588\, T_9^{-1/3})} e^{(10.0837 + 9.530182\, T_9 - 45.8240\, T_9^2 + 102.9940\, T_9^3 - 103.0517\, T_9^4 + 8.19673\, T_9^5)}. \tag{26}$$

In the last expression $\omega\gamma = 1.625 \times 10^{-9}$ MeV and $S(E_0)$ is the astrophysical factor (in MeVb) for the capture through the first resonance calculated at the most effective energy $E_0 = 0.3922 \times T_9^{2/3}$. Note that the first two terms in Eq. (26) determine the contribution from the narrow first resonance while the last term is the contribution from the second resonance and nonresonant contribution.

TABLE III. The low-temperature reaction rates for $^{11}C + p \rightarrow {}^{12}N + \gamma$: temperature in T_9, our adopted reaction rates, and the reaction rates from [14] in cm^3 mole^{-1} s^{-1}.

Temperature (T_9)	Present rates (cm^3 mol^{-1} s^{-1})	Rates from [14] (cm^3 mol^{-1} s^{-1})	Temperature (T_9)	Present rates (cm^3 mol^{-1} s^{-1})	Rates from [14] (cm^3 mol^{-1} s^{-1})
0.01	8.25[−21]	9.43[−21]	0.33	0.012	0.015
0.05	7.55[−10]	8.84[−10]	0.36	0.025	0.030
0.07	3.07[−8]	9.43[−21]	0.37	0.031	0.037
0.10	9.90[−7]	1.19[−6]	0.38	0.038	0.046
0.11	2.33[−6]	2.81[−6]	0.39	0.047	0.056
0.12	4.96[−6]	6.01[−6]	0.4	0.057	0.068
0.13	9.75[−6]	1.19[−5]	0.42	0.083	0.097
0.14	1.79[−5]	2.20[−5]	0.43	0.10	0.12
0.15	3.11[−5]	3.83[−5]	0.44	0.12	0.14
0.16	5.15[−5]	6.40[−5]	0.45	0.14	0.16
0.17	8.20[−5]	1.02[−4]	0.46	0.16	0.19
0.18	1.26[−4]	1.60[−4]	0.47	0.19	0.22
0.19	1.88[−4]	2.40[−4]	0.48	0.21	0.25
0.2	2.74[−4]	3.45[−4]	0.49	0.25	0.29
0.21	3.90[−4]	4.93[−4]	0.50	0.28	0.33
0.22	5.46[−4]	6.93[−4]	0.60	0.83	1.00
0.23	7.54[−4]	9.58[−4]	0.70	1.83	2.26
0.24	0.0010	0.0013	0.72	2.08	2.60
0.25	0.0014	0.0018	0.74	2.35	2.96
0.27	0.0025	0.0031	0.76	2.65	3.35
0.29	0.0047	0.0055	0.78	2.96	3.80
0.31	0.0074	0.0092	0.80	3.29	4.23

VIII. CONCLUSIONS

Low-lying excited states in ^{12}N and ^{13}O were observed through their one- and two-proton decays using the invariant mass method. The states were created via proton-knockout and inelastic interations of an $E/A = 30.3$-MeV ^{13}O beam on a ^{9}Be target. The decay products were detected in a Si-CsI(Tl) ΔE-E multielement telescope.

The known first ($E^* = 0.960$ MeV, $J^\pi = 2^+$) and second ($E^* = 1.181$ MeV, $J^\pi = 2^-$) excited states in ^{12}N were observed via their single-proton decays. The width of the second excited state was determined to 55(20) keV which is significantly smaller than its tabulated value of 118(14) keV.

Two and possibly three new excited states of narrow width ($\Gamma < 50$ keV) were observed in ^{13}O at $E^* = 2.956(20)$, 3.025(16), and 3.669(13) MeV. Either the first of these states undergoes single proton decay while the other two states decay by emitting two protons, or a state near $E^* = 3.0$ MeV has a strong decay branch to the $J^\pi = 2^+$ excited state and a weak branch to the ground state while the high-lying state decays predominately to the second excited state with $J^\pi = 2^-$. As all the excited states of ^{12}N are unbound, the decays to these states emit a second proton to the ground state of ^{11}C. The particle correlations indicate that these two-proton decays are sequential. The decays through the second excited state were also found consistent with the smaller width we measured for this state from the $p + {}^{11}$C events.

Resonance capture via the second excited states of ^{12}N is important for the astrophysical $^{11}C(p,\gamma)^{12}N$ reaction rate. While parts of the R-matrix formalism to treat this reaction was presented previously [14], it was fully presented in the present work and exercised with the new width of the second excited state determined in this work. The substantially reduced width of this state was found to have a modest effect on the reaction rate, reducing it by 26% at $T_9 = 0.2$.

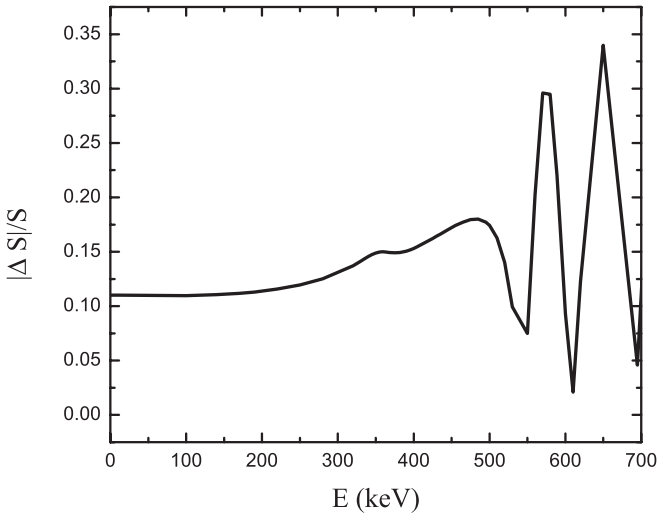

FIG. 7. The total uncertainty of the $S(E)$ factor for $^{11}C(p,\gamma)^{12}N$ reaction calculated using uncertainties of the ANC, the radiative width of the first resonance, and the total width of the second resonance.

ACKNOWLEDGMENTS

We would like to acknowledge a useful conversation with Dr. V. Goldberg concerning the potential structure of the

excited states of ^{13}O. This work was supported by the U.S. Department of Energy, Division of Nuclear Physics under Grants No. DE-FG02-87ER-40316, No. DE-FG02-93ER40773, No. DE-FG52-09NA29467, and No. DE-SC004972. Support is also acknowledged from the National Science Foundation and Natural Sciences and Engineering Research Council of Canada under Grants No. PHY-0852653 and No. 401945-2011, respectively.

[1] P. Couvert, G. Bruge, R. Beurtey, A. Boudard, A. Chaumeaux, M. Garçon, D. Garreta, P. C. Gugelot, G. A. Moss, S. Platchkov, J. P. Tabet, Y. Terrien, J. Thirion, L. Bimbot, Y. Le Bornec, and B. Tatischeff, Phys. Rev. Lett. **41**, 530 (1978).
[2] P. A. Seidl, M. D. Brown, R. R. Kiziah, C. F. Moore, H. Baer, C. L. Morris, G. R. Burleson, W. B. Cottingame, S. J. Greene, L. C. Bland, R. Gilman, and H. T. Fortune, Phys. Rev. C **30**, 1076 (1984).
[3] B. B. Skorodumov, G. V. Rogachev, P. Boutachkov, A. Aprahamian, V. Z. Goldberg, A. Mukhamedzhanov, S. Almaraz, H. Amro, F. D. Becchetti, S. Brown, Y. Chen, H. Jiang, J. J. Kolata, L. O. Lamm, M. Quinn, and A. Woehr, Phys. Rev. C **75**, 024607 (2007).
[4] H. Iwasaki, A. Dewald, C. Fransen, A. Gelberg, M. Hackstein, J. Jolie, P. Petkov, T. Pissulla, W. Rother, and K. O. Zell, Phys. Rev. Lett. **102**, 202502 (2009).
[5] J. B. Ehrman, Phys. Rev. **81**, 412 (1951).
[6] R. G. Thomas, Phys. Rev. **88**, 1109 (1952).
[7] M. Wiescher, J. G. S. Graf, L. Buchmann, and F.-K. Thielemann, Ap. J. **343**, 352 (1989).
[8] G. M. Fuller, S. E. Woosley, and T. A. Weaver, Ap. J. **307**, 675 (1986).
[9] C. L. Fryer, S. E. Woosley, and A. Heger, Ap. J. **550**, 372 (2001).
[10] N.-C. Shu, Y.-S. Chen, K.-S. Wu, X.-X. Bai, Z.-H. Li, and W.-P. Liu, Nucl. Phys. A **758**, 419 (2005).
[11] A. Lefebvre, P. Aguer, J. Kiener, G. Bogaert, A. Coc, F. de Oliveira, J. P. Thibaud, D. Disdier, L. Kraus, I. Linck, S. Fortier, J. A. Scarpaci, C. Stephan, L. Tassan-Got, P. Eudes, F. Guilbault, T. Reposeur, C. Grunberg, P. Roussel-Chomaz, and F. Attallah, Nucl. Phys. A **592**, 69 (1995).
[12] P. Descouvemont, Nucl. Phys. A **646**, 261 (1999).
[13] T. Teranishi, S. Kubono, S. Shimoura, M. Notani, Y. Yanagisawa, S. Michimasa, K. Ue, H. Iwasaki, M. Kurokawa, Y. Satou, T. Morikawa, A. Saito, H. Baba, J. Lee, C. Lee, Z. Fülöp, and S. Kato, Phys. Lett. B **556**, 27 (2003).
[14] X. Tang, A. Azhari, C. A. Gagliardi, A. M. Mukhamedzhanov, F. Pirlepesov, L. Trache, R. E. Tribble, V. Burjan, V. Kroha, and F. Carstoiu, Phys. Rev. C **67**, 015804 (2003).
[15] B. Guo, Z. H. Li, W. P. Liu, and X. X. Bai, J. Phys. G **34**, 103 (2007).
[16] D. W. Lee, J. Powell, K. Peräjärvi, F. Q. Guo, D. M. Moltz, and J. Cerny, J. Phys. G **38**, 075201 (2011).
[17] Evaluated Nuclear Structure Data File (ENSDF) [http://www.nndc.bnl.gov/ensdf/].
[18] C. F. Maguire, D. L. Hendrie, D. K. Scott, J. Mahoney, and F. Ajzenberg-Selove, Phys. Rev. C **13**, 933 (1976).
[19] W. Sterrenburg, M. Harakeh, S. V. D. Werf, and A. V. D. Woude, Nucl. Phys. A **405**, 109 (1983).
[20] C. D. Zafiratos, F. Ajzenberg-Selove, and F. Dietrich, Nucl. Phys. **77**, 81 (1966).
[21] H. Fuchs, K. Grabisch, D. Hilscher, U. Jahnke, H. Kluge, T. Masterson, and H. Morgenstern, Nucl. Phys. A **234**, 61 (1974).
[22] F. Ajzenberg-Selove and C. Busch, Nucl. Phys. A **336**, 1 (1980).
[23] A. Banu, T. Al-Abdullah, C. Fu, C. A. Gagliardi, M. McCleskey, A. M. Mukhamedzhanov, G. Tabacaru, L. Trache, R. E. Tribble, Y. Zhai, F. Carstoiu, V. Burjan, and V. Kroha, Phys. Rev. C **79**, 025805 (2009).
[24] M. F. Jager, R. J. Charity, J. M. Elson, J. Manfredi, M. H. Mahzoon, L. G. Sobotka, M. McCleskey, R. G. Pizzone, B. T. Roeder, A. Spiridon, E. Simmons, L. Trache, and M. Kurokawa, Phys. Rev. C **86**, 011304 (2012).
[25] R. E. Tribble, R. H. Burch, and C. A. Gagliardi, Nucl. Instrum. Methods A **285**, 411 (1989).
[26] R. E. Tribble, C. A. Gagliardi, and W. Liu, Nucl. Instrum. Methods B **56/57**, 956 (1991).
[27] R. Anne, J. Herault, R. Bimbot, H. Gauvin, C. Bastin, and F. Hubert, Nucl. Instrum. Methods B **34**, 295 (1988).
[28] J. F. Ziegler, J. P. Biersack, and U. Littmark, *The Stopping and Range of Ions in Solids* (Pergamon Press, New York, 1985); the code SRIM can be found at www.srim.org.
[29] A. M. Lane and R. G. Thomas, Rev. Mod. Phys. **30**, 257 (1958).
[30] L. V. Grigorenko, T. D. Wiser, K. Mercurio, R. J. Charity, R. Shane, L. G. Sobotka, J. M. Elson, A. H. Wuosmaa, A. Banu, M. McCleskey, L. Trache, R. E. Tribble, and M. V. Zhukov, Phys. Rev. C **80**, 034602 (2009).
[31] R. J. Charity, T. D. Wiser, K. Mercurio, R. Shane, L. G. Sobotka, A. H. Wuosmaa, A. Banu, L. Trache, and R. E. Tribble, Phys. Rev. C **80**, 024306 (2009).
[32] B. B. Back, S. I. Baker, B. A. Brown, C. M. Deibel, S. J. Freeman, B. J. DiGiovine, C. R. Hoffman, B. P. Kay, H. Y. Lee, J. C. Lighthall, S. T. Marley, R. C. Pardo, K. E. Rehm, J. P. Schiffer, D. V. Shetty, A. W. Vann, J. Winkelbauer, and A. H. Wuosmaa, Phys. Rev. Lett. **104**, 132501 (2010).
[33] S. Baroni, P. Navrátil, and S. Quaglioni, Phys. Rev. Lett. **110**, 022505 (2013).
[34] S. Baroni, P. Navrátil, and S. Quaglioni, arXiv:1301.3450.
[35] S. K. Bogner, R. J. Furnstahl, and R. J. Perry, Phys. Rev. C **75**, 061001 (2007).
[36] R. Roth, S. Reinhardt, and H. Hergert, Phys. Rev. C **77**, 064003 (2008).
[37] R. Roth, T. Neff, and H. Feldmeier, Prog. Part. Nucl. Phys. **65**, 50 (2010).
[38] D. R. Entem and R. Machleidt, Phys. Rev. C **68**, 041001 (2003).
[39] P. Navrátil *et al*. (unpublished).
[40] F. C. Barker and T. Kajino, Aust. J. Phys. **44**, 369 (1991).
[41] R. J. Holt, H. E. Jackson, R. M. Laszewski, J. E. Monahan, and J. R. Specht, Phys. Rev. C **18**, 1962 (1978).
[42] F. Ajzenberg-Selove, Nucl. Phys. A **506**, 1 (1990).
[43] T. Minemura *et al*., RIKEN Accel. Prog. Rep. A **35**, 58 (2002).